Biophysical Chemistry, 32 (1988) 211–227
Elsevier

BPC 01327

The internal dynamics of gene 32 protein–DNA complexes studied by quasi-elastic light scattering

M.E. Kuil, F. van Mourik, W. Burger and R. van Grondelle

Department of Biophysics, Free University, De Boelelaan 1081, 1081 HV Amsterdam, The Netherlands

Received 29 May 1988
Accepted 28 September 1988

DNA-protein interaction; Internal dynamics; Macromolecular flexibility; Hydrodynamic parameters; Quasi-elastic light scattering; Global analysis

The hydrodynamic properties of large homodisperse single stranded DNAs complexed with the helix destabilizing protein of phage T4, the product of gene 32 (GP32), have been measured. The results suggest a size of the binding site between 8 and 10 nucleotides/GP32 molecule, in reasonable agreement with earlier work on a complex between GP32 and single stranded 145 base DNA. From static light scattering experiments it is concluded that the persistence length of these complexes is about 30 nm, distinctly smaller than the generally accepted value for double stranded DNA. The quasi-elastic light scattering properties of the DNA–GP32 complexes were determined. The variation of the apparent translation diffusion coefficient D_{app} with the scattering vector q was analyzed using the discrete ISMF and Rouse-Zimm models [S.C. Lin et al., Biopolymers 17 (1978) 425]. The model parameters that followed from the fit of D_{app} versus q^2 and from an extensive global analysis of the actually measured autocorrelation functions agreed with the notion that these DNA–protein complexes are indeed rather flexible. The continuous Soda model [K. Soda, Macromolecules 17 (1984) 2365] could successfully explain the variation of D_{app} versus q^2, assuming a persistence length of 30 nm and a base–base distance in the complex of 0.44 nm.

1. Introduction

Gene 32 protein (GP32) encoded by the DNA of bacteriophage T4 is essential for the replication of the phage DNA after infection of the host bacterium *Escherichia coli* [1]. The protein plays an important role in the replication and repair of T4-DNA [2]. The specific structure of the complexes formed after binding of GP32 to single stranded (ss) DNA is thought to be essential for the special role that the protein plays in these processes [3].

Several investigators have studied the binding of GP32 to ss DNA using a variety of different techniques [4–6]. The thermodynamics of the binding of the protein to ss DNA is well described by three parameters: the intrinsic binding constant K_{int}, the cooperativity constant ω and the size of the binding site, n. The cooperativity parameter ω is estimated to be $1–5 \times 10^3$ and the size of the binding site, n, ranges from 5 to 11 nucleotides covered by one protein molecule [5,7]. The intrinsic binding constant is strongly salt dependent, being maximal at an ionic strength of 50 mM. Recently, Scheerhagen et al. [8] established the structural parameters that can be ascribed to the ss DNA–GP32 complex by using a combination of optical and hydrodynamical techniques. It was shown that the solution dimensions of the ss 145 base DNA fragment changed drastically upon complexation with GP32. From the electric field birefringence decay it was calculated that the base–base distance projected along the long axis of the complex was at least 0.44 nm per nucleotide [9]. This value compared rather well with the value of 0.46 nm per nucleotide determined by electron microscopy [10]. The size of the binding site was determined by combining the sedimentation and

0301-4622/88/$03.50 © 1988 Elsevier Science Publishers B.V. (Biomedical Division)

the translation diffusion coefficient using the Svedberg relation, and was found to be 10 nucleotides covered per protein monomer. The hydrodynamic results together with optical data and calculations of absorption and circular dichroism spectra resulted in a rather detailed picture of the average conformation of ss DNA–GP32 complexes [12]. Recently, linear dichroism experiments further substantiated this proposed averaged conformation for several synthetic polynucleotides as well as for natural DNAs, including the 145 base DNA in complex with GP32 [13,46]. In this work we study the structural fluctuations in large DNA GP32 complexes using both classical and dynamic light scattering. Theories have been advanced that relate the observed scattered light intensities and autocorrelation functions to a set of parameters that can be discussed in terms of flexibility [14]. A summary of these theories will be presented below. All the results indicate that the structural properties that characterize the long DNA–GP32 complexes are very similar to those of the short complex. In addition, the GP32–ss DNA complexes must be rather flexible.

2. Materials and methods

2.1. General

All chemicals used were reagent grade. All hydrodynamic parameters were measured at a temperature close to 20 °C, and corrected to the standard temperature of 20 °C. The buffer used in all experiments was 2 mM Na_2HPO_4, 0.2 mM Na_2EDTA and 50 mM NaCl with pH 7.2.

2.2. Protein preparation

GP32 was purified essentially as described by Moise and Hosoda [18]. *E. coli* BE-cells were infected with the overproducing triple mutant T4*amN*134(33)*amB*292(55)*amE*219(61) (both strains were a kind gift of Dr. Hosoda, University of California, Berkeley, U.S.A.). GP32 eluted with a 2 M NaCl wash of the ss DNA agarose column was applied to a G-75 Sephadex (Pharmacia, Sweden) column to remove most of the proteolytic activity. Preequilibration of this column with 0.1 M NaCl buffer allowed us to apply the eluate directly on a DEAE-cellulose column. The protein was eluted with a 0.1–0.6 M NaCl salt gradient and eluted at a salt concentration of 0.2 M NaCl. The protein was stored immediately after purification at 3–5 mg/ml concentration at −20 °C. As shown by polyacrylamide gel electrophoresis the GP32 protein was at least 90% pure.

2.3. DNA preparation

2.3.1. Plasmid pBR322

Plasmid pBR322 harbouring *E. coli* C 0 bacteria were grown on ampicillin containing medium. Cell lysis was performed using the 'cleared lysate' method [19]. The plasmid was banded on a CsCl-gradient (44 h, 38 000 rpm) and collected by side-puncturing the centrifuge tube after visualization of the plasmid using ethidium bromide (Sigma) with long-wavelength UV light. After extensive extraction of the ethidium bromide with iso-propanol followed by dialysis the material was treated with RNAse (Worthington). The material was extracted with freshly distilled phenol (Baker) and after dialysis the DNA was precipitated with pure ethanol (Baker) and resuspended. Incubation with *Eco*RI (Boehringer) restriction endonuclease in the recommended buffer for 30–60 min at 37 °C was used to obtain a linear molecule. The completion of the digestion was confirmed using 1% agarose gel electrophoresis. A final protein extraction with fresh phenol and an ethanol precipitation had been performed before the DNA was stored at −20 °C.

2.3.2. Phage DNA

Phage λ-DNA (λ*c*I857*Sam*7) was purchased from Boehringer (Mannheim, F.R.G.) and was used without further purification. Phage M 13-DNA was a kind gift of Dr. B.J.M. Harmsen (Catholic University of Nijmegen, The Netherlands). M 13mp 10 phages were grown on *E. coli* JM 101 and the DNA was extracted from purified phage particles using standard procedures [19]. All the phage DNAs migrated as a single band on 1% agarose gels.

2.3.3. Nucleosome DNA

Double stranded nucleosomal DNA was prepared using the method described by Lutter [20]. The material was homodisperse in length as judged by the field strength and duration dependence of the decay of the electric birefringence signal as described elsewhere [9]. In addition the homogeneity was checked using a 6% polyacrylamide gel with a low molecular weight DNA marker.

2.4. Sedimentation

Ultracentrifuge experiments were performed using a MSE centriscan 75 ultracentrifuge equipped with a UV-absorbance scanner. The rotor speed in these experiments ranged from 18 000 to 24 000 rpm and the rotor temperature was kept at 20 °C by the built-in temperature controller. The position of the sedimenting boundary was taken at halfheight of the plateau. Since the boundary was quite steep this method introduces only a slight error. The sedimentation coefficients were calculated by applying a least squares method. The logarithm of the boundary position varied linearly with the sedimentation time for all rotor speeds used.

2.5. Absorbance measurements

A description of the absorbance spectrophotometers and titration technique is given by Van Amerongen et al. [15]. The titrations were performed at a temperature of 11 °C maintained by a Lauda thermostat bath. The absorbance data were transferred to a VME131 computer system for further data analysis.

Calculation of the interaction spectrum. In the titration experiments a dilute DNA solution was titrated with small aliquots of a concentrated protein solution. After weighing the amount of added protein and gently mixing of the components an absorbance spectrum was recorded from 240 to 420 nm. We assume that the obtained spectrum consists of three contributions, i.e. the DNA spectrum, the protein spectrum and an 'interaction' spectrum; the last spectrum can be calculated. When the long ss DNA was complexed with GP32 in this type of experiment an increased absorbance in the 350–420 nm region could be observed in the 'interaction spectrum' which was absent when we used nucleosomal ss DNA. Since none of the components significantly absorbs light in this wavelength region, we ascribe this change to the formation of large, high molecular weight structures. The absorbance change in this region of the spectrum can be fitted to the following relation

$$\Delta A = C\left[\frac{\lambda}{\lambda_0}\right]^{\gamma} + B \qquad (1)$$

where C is a proportionality constant, B an offset and λ_0, a reference wavelength (in this case chosen to be 420 nm). The obtained correction was used to calculate the scattering corrected 'interaction spectra' between 240 and 350 nm.

2.6. Light scattering

2.6.1. Sample preparation

If necessary we denatured the double stranded DNA by heating to 95 °C followed by a rapid chill on ice. After the sample had reached a temperature of about 30 °C an aliquot of ice-cold GP32 solution was added and gently mixed with the DNA. In all cases excess protein was added to the DNA solution using a conservative estimate of the size of the binding site to obtain a fully saturated complex. We typically used a DNA concentration of $\approx 25\ \mu g/ml$ in all experiments. Since sample purity is essential for light scattering we used a combination of filtration and gel exclusion chromatography to remove unwanted particles. First the freshly prepared protein–DNA complex was applied to a G-100 Sephadex (Pharmacia) column to remove excess protein that might aggregate during the experiment. Next the eluate was filtered using Millipore filter (Sartorius) with an appropriate pore diameter, e.g. 0.2 μm for pBR322 and M 13 and either 0.45 μm or 1.2 μm for M 13mp 10 and λ DNA. The filtrate was led directly into a scattering cell, which had been rinsed using acetone vapour and sealed with Parafilm after the acetone had evaporated. The formation of a saturated complex was checked using CD spectroscopy.

2.6.2. Setup

We performed homodyne quasi-elastic light scattering (QELS) experiments using an Argon-ion laser (Spectra Physics model 165) equipped with either visible or UV optics. The scattered light was detected using a FW130 photomultiplier (EMI) followed by an amplifier discriminator (Ortec 9302). The photon pulses were fed into a Malvern K7023 (96 channels) correlator after passing a home-built pulse shaper to meet the input specifications of the correlator. This setup has been described in more detail elsewhere [21]. The sample interval of the correlator was adjusted to have about 8 decay times in the measured time domain, to allow for good estimates of very slight baseline shifts. We used typically 50–200 mW light intensities at 488.0 or 514.5 nm and about 10 mW at 351.1 nm for the light scattering experiments. The classical light scattering experiments were performed using 514.5 nm light which gave the best intensity stability. Within error of the experiment all reported data did not depend on the laser intensity. Laser intensity drift (e.g. 'mode hops' and temperature changes of the oscillator) can result in an incorrect normalisation of the obtained autocorrelation function. It proved to be convenient to do many short measurements (1–10 s each) to obtain a more correct normalisation. In this manner we could also observe the fluctuations in the average number of photoncounts and examine the effect of rejection of both high and low countrates from the average. If an occasional larger particle had entered the beam either in front or behind the scattering volume the measured correlation function was rejected from the result, if the fluctuation was greater than $10\sqrt{n}$, with n the mean countrate per second for all experiments. Typically 1–5% out of 400 measurements of 1 s was rejected. During a long measurement with only a small count rate the 'normalisation' in the usual fashion is largely affected by a spurious 'Tyndall' fluctuation, and has to be repeated. This disturbance usually lasts for only a few seconds and can be deleted easily by rejection of some individual curves from the measured data set. However, when more than 10–20% of the recorded curves had to be rejected it was clear that the sample quality was too poor to perform useful measurements at all.

To measure the particle-interference function for the various DNA–protein complexes, we calibrated the QELS setup using a solution of latex spheres of known size. Latex spheres with a diameter around 100 nm ensured that the scattered intensities of the sample and reference were of comparable magnitude. Aggregation in the reference solution could easily be detected using the obtained autocorrelation function. The scattered intensities of the latex spheres were compared with those of the DNA–protein complex and thus the angular dependence of the scattering volume was eliminated. The experiments directly yielded the desired particle interference function for the DNA–protein complex, apart from a normalizing constant. An internal control was performed using latex spheres of a rather different size, yielding the correct radius of gyration within an error bound of less than 10%.

2.6.3. Data analysis

We used two approaches to obtain the model parameters from the quasi elastic light scattering data:

(i) D_{app} versus q^2. All autocorrelation functions C were first fitted to $A \exp(-2D_{app} q^2\tau) + B$, where q^2 is the squared magnitude of the scattering vector $\boldsymbol{q}$ given by $4 \pi n \sin(\theta/2)/\lambda$ with n the refractive index of the solution, θ the angle between the incoming and scattered beam and λ the wavelength used. D_{app} is the apparent diffusion coefficient, A the amplitude of the correlation function and B is an offset. Hereby homodyne detection of the scattered light is assumed. As can be seen from the analytic expression used (see theory; eq. 5) this method is essentially not correct. Except for the smallest scattering angles we do not expect the autocorrelation functions to be single exponential. However, we assume that the obtained apparent diffusion coefficient can be related to the first cumulant of the theoretical expressions used [14,25]. The values of D_{app} at different values of the scattering vector $\boldsymbol{q}$ were ordered in pairs (D_{app} and q^2) and the following sum was minimized:

$$U = \sum_{j=1}^{K} \left[D_{app}(\exp)(q_j) - D_{app}(\mathrm{th})(q_j) \right]^2 \qquad (2)$$

Several different expressions for the theoretical value of D_{app} were used, which will be introduced in the next section.

(ii) Global analysis. As indicated above the method used for the analysis of the D_{app} versus q^2 is strictly spoken incorrect. To overcome this problem we performed a global analysis and the autocorrelation-functions obtained with four to six different values of q^2 were fitted simultaneously using the dynamic structure factor of an appropriate molecular model. In this approach we minimize the following sum:

$$R = \sum_{j=1}^{M} \sum_{i=2}^{96} \left[C(q_j, \tau_i) - c_i | S(q_j, \tau_i) |^2 \right]^2 \qquad (3)$$

The dynamic structure factor $S(q, \tau)$ was calculated according to eq. 5 with an appropriate choice of one of the functions A_i defined in eqs. 6, 7 or 8 (see section 3). The number of unknown parameters is equal to the number of model parameters plus the number of q^2 values included, since we apply individual normalizing factors, c_i for each correlation function. The number of data points is equal to the total number of points, 95, in a single autocorrelation function times the number of q^2 values used (M). In general, there are $M+3$ unknowns and 95 M data points since from all correlation functions the first data point was routinely omitted. If more than one autocorrelation function is included in the global analysis the number of unknowns is smaller than in (i) since no offset is included in the latter approach.

3. Theory

To describe the obtained autocorrelation functions we used several models applicable to the dynamics of wormlike chains. We introduce the models shortly with some references to applications on double stranded DNA in the next sections.

3.1. The ISMF model [24]

In this model n_0 ($= N+1$) segments of a molecule diffuse independently in a radial harmonic potential with a strength g which is adjusted to give the correct radius of gyration (R_g) of the molecule. Every segment has an isotropic translation friction factor f. A remarkable feature of this model is that the segments of the molecule are not physically connected. The ISMF model has been used for a description of the internal dynamics of calf thymus DNA [14]. We apply it to fit our data of GP32 complexed with linear and circular DNAs.

3.2. The Rouse-Zimm model [14,25]

In this model $N+1$ beads are connected with identical ideal springs with a spring constant g. The individual beads have a translational friction coefficient f. The spring constant g determines the root mean square distance between the beads. The Rouse-Zimm model was used extensively to describe the internal dynamics of double stranded DNAs such as calf thymus, $\phi 29$ and λ DNA. It was shown that a universal choice of the parameter set was possible, with the appropriate scaling, for DNAs of various lengths [26]. Moreover, the temperature independence of the model parameters was demonstrated [25]. We used both the linear and circular free draining chain formulas in the calculation of the autocorrelation functions.

To calculate the autocorrelation function we need an expression for the dynamic structure factor $S(q, \tau)$ with q the scattering vector and τ the time in q space. The autocorrelation function is given by:

$$C = | S(q, \tau)^* S(q, \tau) |^2 \qquad (4)$$

in which $S(q, \tau)^*$ is the complex conjugate of $S(q, \tau)$. The expressions for the two discrete models above can be generalized into one formula:

$$S(q, \tau) = (N+1) \exp\left(-q^2 \left(D_0 - \frac{k_B T}{f(N+1)} \right) \tau \right) \times \left[\exp\left(-q^2 \frac{k_B T}{f} \tau \right) + A_i(q, N, g, T) \right] \qquad (5)$$

where $D_0 - k_B T/(N+1)f$ is the diffusion coefficient of the whole molecule which can be obtained in the limit $q \to 0$. k_B is Boltzmann's constant, T

is the absolute temperature. The functions A_i are dependent on the choice of a model but independent of τ.

For the ISMF model we have:

$$A_{\text{ismf}} = N \exp\left(-q^2 \frac{k_B T}{g}\right) \tag{6}$$

For the linear Rouse-Zimm chain:

$$A_{\text{lrzc}} = \sum_{n=1}^{N+1} \sum_{\substack{p=1 \\ p \neq n}}^{N+1} \frac{\exp\left(-q^2 (k_B T/g)\,|n-p|\right)}{N+1} \tag{7}$$

And for the circular Rouse-Zimm chain:

$$A_{\text{crzc}} = \sum_{r=1}^{N} \exp\left(-q^2 \frac{k_B T}{2g}(N+1)\frac{r}{N+1} \times \left\{1 - \frac{r}{N+1}\right\}\right) \tag{8}$$

3.3. The Soda model for circular wormlike chains

The theory of Soda [16] is very attractive to apply to the DNA–protein complexes because the bending persistence length is explicitly included as one of the model parameters. Although it is known that the longitudinal stiffness is treated in an incomplete way, the model gives rather good predictions for the static light scattering properties of the wormlike ring [16], including hydrodynamic interaction. Moreover, the model has been successfully applied to experiments with the plasmid ColE1 [17]. Since we determined both the dynamic and static light scattering properties of two circular covalently closed DNA–protein complexes and because we are specifically interested in an estimate of the persistence length of the DNA–protein complexes the theory of Soda seems well suited for our purpose.

The discrete Berg chain [29] is the starting point for the Soda theory. It is transformed to a continuous chain by increasing the number of beads and keeping the contour length L fixed. A general expression for the dynamic structure factor is given by:

$$S(q, \tau) = 2L\alpha^2 \exp\left(-D_0 q^2 \tau\right) \int_0^{L/2} ds\, c(q, s, \tau) \tag{9}$$

where D_0 is the translation diffusion coefficient and α is the polarizability per unit length. $c(q, s, \tau)$ is integrated along the chain using the reduced variable s. The function $c(q, s, \tau)$ is given by:

$$c(q, s, \tau) = \exp\left[-\sum_{n=1}^{\infty} \frac{4k_B T q^2}{3L\lambda_n}\left(1 - \cos\left(\frac{2\pi n s}{L}\right) e^{-\tau/\tau_n}\right)\right] \tag{10}$$

where λ_n is a function of the flexibility of the chain and τ_n is the relaxation time of the n-th normal mode. The hydrodynamic interaction, included in the value of τ_n, is determined by ξ_n/λ_n. ξ_n is the friction coefficient of the n-th normal mode, which contains the hydrodynamic interaction, and ξ_n can be calculated given a appropriate choice for the molecular diameter using an expression for the mean reciprocal distance between two segments on the contour of the molecule (see eq. 10 in ref. 22 and eq. 50 in ref. 16).

3.4. D_{app} versus q^2

To describe the D_{app} versus q^2 curve we used three models to calculate D_{app}: (i) the first cumulant for a linear Rouse-Zimm chain with hydrodynamic interaction [25]; (ii) the first cumulant for the ISMF model; (iii) an autocorrelation function was calculated using eqs. 9 and 10. Subsequently this function was analyzed in a similar way to our experimental data thus yielding a value for D_{app} for a given value of q^2.

3.5. Intra-particle interference

The intra-particle interference factor $P(\theta)$ was calculated using a formula given by Peterlin [23], which is incorrectly generalized in ref. 27:

$$P(\theta) = e^{p}\left[\sum_{m=0}^{\infty} \frac{(-p)^m}{m!} F((p+m)x)\right] \tag{11}$$

with

$$F(y) = \frac{2}{y^2}(y - 1 + e^{-y})$$

and $x = L/a$ and $p = q^2 a^2/3$. Adjustable parameters in this expression are the bending persistence length a and the contour length L of the molecule.

All models described above were implemented on a VME131 micro-computer and were calculated using double precision arithmetic.

4. Results

4.1. Absorbance titrations

To compare the saturation of both a large and small DNA with GP32, absorbance titrations were performed. In figs. 1 and 2 we show the calculated 'interaction spectra' for the M 13mp 10 and 145 base ss DNA complexed with GP32 respectively. Upon addition of a saturating amount of GP32 these interaction spectra seem to reach a 'final' spectrum, indicating that there is no further interaction after saturation is reached. To estimate the size of the binding site we plotted the absorbance change at 260 nm versus the concentration of protein in the insets of figs. 1 and 2. The binding site size of GP32 on M 13mp 10 was calculated using an extinction coefficient of 37×10^3 M^{-1} cm^{-1} at 280 nm for GP32 [42] and an extinction coefficient of 7400 M^{-1} cm^{-1} at 259 nm for M 13mp 10 [43] yielding a value of 6.8 ± 0.5 nucleotides covered by one protein monomer. A value of 7.1 ± 0.5 nucleotides covered by one protein monomer was calculated for the 145 base DNA complex, using the same extinction coefficients. The absorbance changes for both complexes compare very well, confirming that the extent of saturation is the same for both complexes. Typically a value of γ between -3 and -4 was found for the exponent in the scattering correction procedure (see eq. 1), indicative of an extended structure. We note that the size of the binding site is not influenced by the scattering correction since this correction was proportional to the saturation of the complex. The total contribution of the scattering correction at 260 nm was less than 0.04 A units.

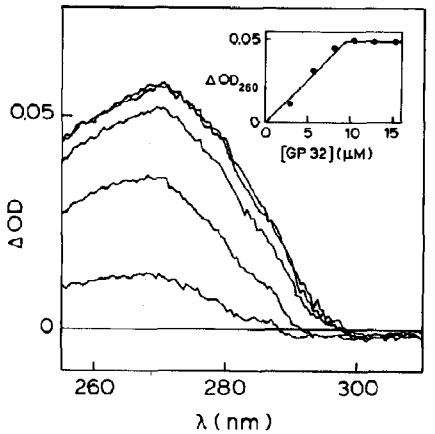

Fig. 1. Absorbance difference spectra after addition of GP32 (136 μM) to M 13mp 10 (54 μM) DNA. The spectra were corrected for dilution and for scattering as described in the text. Both the protein and DNA contribution have been subtracted. Inset: absorbance changes at 260 nm versus the total protein concentration.

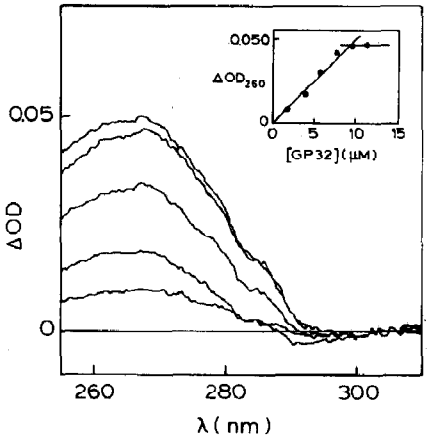

Fig. 2. Absorbance difference spectra after addition of GP32 (136 μM) to ss 145 base DNA (60 μM). The spectra were corrected for dilution and scattering as described in the text. Both the protein and DNA contribution have been subtracted. Inset: absorbance changes at 260 nm versus the total protein concentration.

4.2. Sedimentation

Boundary sedimentation experiments were performed with four long ss DNA molecules complexed with GP32. Linearized plasmid pBR322 DNA was heat denatured before complexation with GP32. Fig. 3 shows some representative ab-

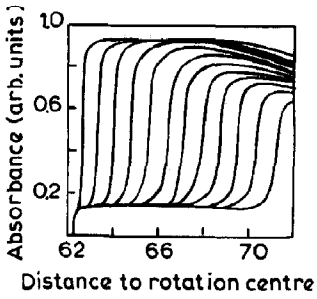

Fig. 3. Sedimentation profiles recorded every 10 min of GP32 complexed with ≈ 25 μg/ml pBR322, using the UV-scanner. The least squares fit resulted in a value of 54 S for $s_{20,w}$. The rotor speed was 18000 rpm and the temperature was 20 °C during the run.

sorbance scans taken during the sedimentation run that was performed with pBR322 complexed with GP32. From the steep boundary it was inferred that a rather narrow distribution of DNA molecules covered with (cooperatively) bound protein was sedimenting. The sedimentation coefficient that can be calculated from the shift of the boundary position at early times during the run compared very well with the boundary position at the end of the run. Moreover, similar observations were made with M 13 and M 13mp 10 DNA complexes. Rather different results were obtained from sedimentation experiments with λ DNA: no single steep boundary was observed which was probably caused by the introduction of single strand breaks in the λ DNA during the denaturation procedure. These complexes gave a similar circular dichroism spectrum to the other DNA–protein complexes, so the DNA must be saturated with GP32. In table 1 the sedimentation coefficient and the translational diffusion coefficient obtained from small angle QELS experiments (see section 4.4) for the three shortest DNAs are presented. For comparison the translational diffusion coefficient and a calculated value for the sedimentation coefficient for linearized double stranded pBR322 DNA are shown. Comparing this experimental value for the translational diffusion coefficient of double stranded DNA with the value found for the complex it can be noted that the diffusion coefficient has decreased by almost 20%. Since the translational diffusion coefficient is weakly dependent on the molecular diameter this observation is indicative of a 40% increase in the molecular length assuming that the translational diffusion coefficient is inversely proportional to the square root of the contour length for molecules of this length, and that both molecules have a comparable flexibility. The large value of the sedimentation coefficient of pBR322 complexed with GP32 ($s_{20,w} = 50$ S) compared with double stranded pBR322 shows that indeed a DNA–protein complex with a high molecular weight has been formed; the same conclusion holds for the other DNA–protein complexes. The molecular weights can be calculated using the Svedberg relation with the assumption of a reasonable value for the partial specific volume. Since about 90% of the mass of the complex consists of GP32 we used the partial specific volume of the protein (0.73 g/cm^3) [30]. In the last column the calculated size of the binding site for all three homodisperse DNA–protein complexes is given together with values mea-

Table 1

Hydrodynamic parameters and size of the binding site

Type of DNA complexed with GP32	No. of bases	$s_{20,w}$ (10^{-13} s^{-1})	$D_{20,w}$ (10^{-12} m^2 s^{-1})	M_w (10^3 mol/kg)	Size of the binding site
145 bp [a]	145	11.6	19.1	0.54	10.0
pBR322	4363	50	2.2	20.5	7.7
M 13	6407	61	2.21	24.9	9.4
M 13mp 10	7229	85	2.75	27.9	9.5
ds pBR322	2×4363	14.1 [b]	2.60	2.8	

[a] These data were taken from ref. 9.

[b] This value was calculated using a molecular weight of 2.88×10^3 mol/kg in the empirical relation given by Crothers and Zimm [28].

sured by Scheerhagen et al. using 145 base DNA–protein complexes [9]. The values found for both M 13 DNA complexes, $n = 9.4$ and $n = 9.5$ respectively, are only slightly lower than the number reported by Scheerhagen et al. [9] for the much smaller 145 base DNA–GP32 complex, using the same approach. The number for the pBR322 complex is significantly lower, but in our opinion less accurate than the two M 13 values, in view of the inaccuracy of the D_t value at low scattering angles (see below) and the relative small number of experiments for this complex. However, we cannot exclude the possibility that for the pBR322 GP32 complex the value of n is truly smaller than for the two other complexes.

4.3. Classical light scattering

Light scattering measurements were performed with three DNAs, complexed to GP32. From such measurements the intra-particle interference factor $P(\theta)$ could be obtained for the DNA–protein complexes by direct comparison of the scattered intensity with a standard latex solution. The experimental data points were directly fitted to eq. 11 with as adjustable parameters the bending persistence length a and the contour length L of the molecule. Since we do not know the correct normalization for the $P(\theta)$ function for the DNA–GP32 complex we had to include a normalization factor which introduces one extra variable. From the obtained persistence length and contour length one can calculate the radius of gyration of the molecule using:

$$R_g = \left[aL \left\{ \frac{1}{6} - \frac{a}{2L} + \frac{a^2}{L^2} - \frac{a^3}{L^3}\left(1 - e^{-L/a}\right) \right\} \right]^{1/2}$$

The shape of the $P(\theta)$ function is strongly influenced by the value of the radius of gyration, and it seems possible to estimate this parameter within an error of about 10%. However, the dependence of $P(\theta)$ on the persistence length and the contour length is strongly correlated, e.g. several choices of these two parameters could give a good fit of the data. To obtain a more reliable estimate of the persistence length we constrained the contour length using a probable rise per base

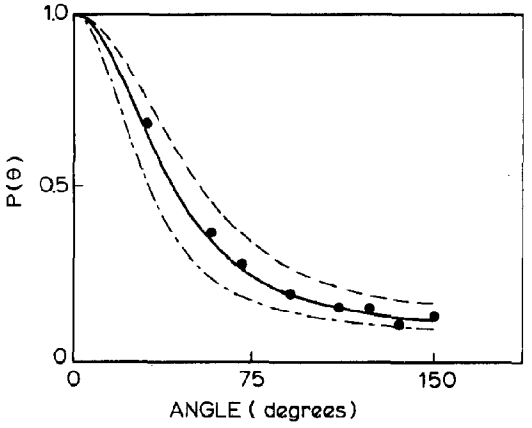

Fig. 4. The intra-particle interference factor $P(\theta)$ of ss pBR322 complexed with GP32 measured at different scattering angles. The drawn line represents a best fit with a constrained contour length of 1920 nm, yielding a persistence length of 33 nm. $P(\theta)$ functions calculated with the same contour length and persistence lengths of 20 and 60 nm are drawn as dashed and dashed dotted lines for comparison.

of 0.44 nm estimated from the measured rotational diffusion coefficient of the 145 base DNA–GP32 complex [9]. Since we know exactly the number of nucleotides incorporated in the DNAs used, we can describe the $P(\theta)$ data with two free parameters, a and the normalization for each complex. To give an impression of the variability the calculated $P(\theta)$ is shown in fig. 4 for several choices of the persistence length. In fig. 4 we show the measured $P(\theta)$ function for the complex of pBR322 with GP32 assuming a contour length for this DNA–protein complex of 1920 nm. In fig. 5 we co-plotted the data points for M 13 and M 13mp 10 GP32 complexes. The experimentally determined $P(\theta)$ functions can be well described by eq. 11. The calculated persistence length, assuming a fixed rise per base, is the same for M 13 and pBR322 and coincides rather well with that estimated on the basis of the theory of Soda (next section). The persistence length calculated for the M 13mp 10 was even smaller, although the spectroscopic properties of this complex were identical to those observed for M 13. In all cases the persistence length of the DNA–protein complex was significantly smaller than that reported for double stranded DNA ($\approx$ 50

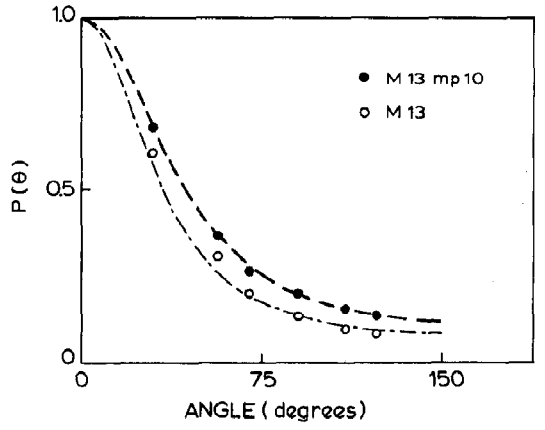

Fig. 5. $P(\theta)$ of GP32 complexed with either M 13 or M 13mp 10 measured at different scattering angles. Best fits were calculated using constrained values for the contour length of 2820 nm for M 13 and 3180 nm for M 13mp 10, yielding persistence lengths of 32 nm and 17 nm respectively.

nm [31]). These results clearly indicate that the DNA–protein complex is a rather flexible structure, contrary to our original ideas [9,11]. The M 13mp 10 DNA in complex with GP32 seems clearly more flexible than the M 13 and pBR322 complexes. These results therefore suggest that sequence effects may play a role in determining the actual structure of these complexes.

In table 2 we summarize the obtained persistence lengths and radii of gyration for the different complexes together with the chosen contour lengths which were fixed during the fit of $P(\theta)$ to the data points.

Table 2

Radii of gyration and persistence lengths from $P(\theta)$ measurements

Type of DNA complexed with GP32	Contour length [a] (nm)	Radius of gyration (nm)	Persistence length [b] (nm)
pBR322	1920	141	33
M 13	2820	170	32
M 13mp 10	3180	133	17

[a] The fixed contour length was calculated using a rise per base of 0.44 nm, yielding a best value for the persistence length.

[b] This value is an upper limit, since the actual rise per base might be greater [9].

4.4. Quasi elastic light scattering

The angular dependence of the apparent diffusion coefficient was studied for three different DNAs complexed with GP32. The plasmid pBR322 DNA was linearized with the *Eco*RI restriction enzyme prior to the experiments to prevent fast renaturation of the molecule. In fig. 6 the apparent diffusion coefficient as obtained from a single exponential plus baseline fit is plotted for different values of the squared length of the scattering vector q^2. The experimental data show a quasi saturation at a level of about 7×10^{-12} m^2 s^{-1} at $q^2 = 20 \times 10^{-14}$ m^{-2}. Note the absence of a distinct plateau at low q^2 values. Although measurements at smaller scattering angles (lower than 30°) would have given more detailed information, the quality of the samples did not permit this. In fig. 7 we show a similar set of data obtained for the circular complexes of M 13 and M 13mp 10 DNA with GP32. These measurements give a somewhat lower value for D_{app} at large values of q^2. At large values of q^2 the spatial fluctuations probed by QELS are of the order of 25–50 nm and differences in the contour length are expected to contribute very little to the observed diffusion coefficient. For small values of q^2 the appearance of a region where D_{app} is fairly constant indicates that the internal dynamics of

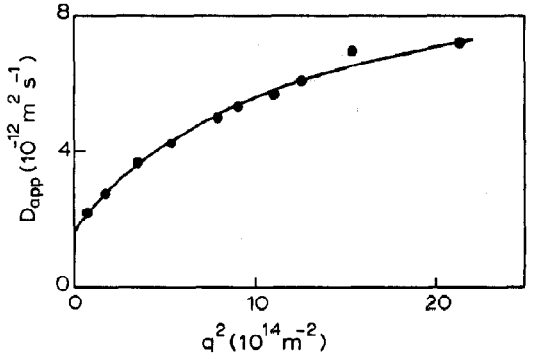

Fig. 6. The apparent diffusion coefficient versus q^2 for pBR322 complexed with GP32. The curve through the data points is a best fit using eq. 9 from ref. 25. A best fit for $N = 40$ was obtained for $D_{plat} = 8.1 \times 10^{-12}$ m^2 s^{-1} and D_0, the small angle diffusion coefficient of 1.6×10^{-12} m^2 s^{-1}. The radius of gyration that can be calculated from these data points is 184 nm.

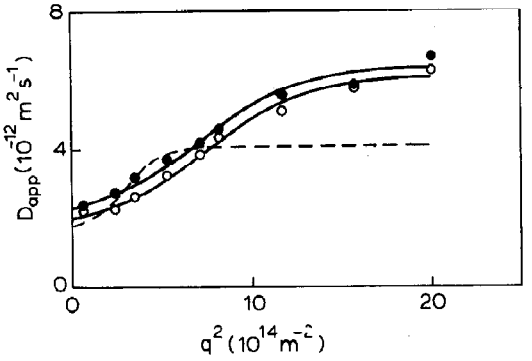

Fig. 7. The apparent diffusion coefficient versus q^2 for M 13 (○) and M 13mp 10 (●) DNA complexed with GP32. The drawn lines represent a best fit obtained with the ISMF model. The best estimates for M 13 complexes (lower curve) are: $D_0 = 2.05 \times 10^{-12}$ m^2 s^{-1}; $R_g = 103$ nm and $kT/f = 4.3 \times 10^{-12}$ m^2 s^{-1}. For M 13mp 10 complexes (upper curve) these parameters were estimated as: $D_0 = 2.27 \times 10^{-12}$ m^2 s^{-1}, $R_g = 106$ nm and $kT/f = 4.3 \times 10^{-12}$ m^2 s^{-1}. The dashed line is a 'fit' using a constrained ISMF model with a fixed R_g of 171 nm with $N = 20$.

the molecule play a smaller role than for the linear DNA at comparable values of q^2. It seems likely that some of the internal motions of the circular chain are damped due to the fact that the two ends of the molecule are connected. Since this initial plateau is observed for both circular DNAs and not for the linear DNA we conclude that this feature is uniquely associated with the circular nature of the molecule. A similar conclusion was drawn by Voordouw et al. [31] who measured D_{app} at small angles for supercoiled circular (relaxed form) and linear plasmid ColE1 DNA. Their data show that the most restricted molecule (supercoiled) has the largest plateau, whereas the plateau is nearly absent for linear DNA. The relaxed form of ColE1 DNA shows an intermediate behaviour in the low q^2 region. Analogous observations have been made by Langowski et al. [32] in their study of supercoiled and linear pUC8 plasmid DNA.

To quantify our observations we described the D_{app} versus q^2 curves with three different model curves, the expression used by Schurr et al. to describe linear DNA with hydrodynamic interaction included (or the Rouse-Zimm model) [14], the ISMF model [24] and the expression given by Soda et al. [16] (see section 3). We found that the Rouse-Zimm model could well describe the curves found for the linear DNA. The best fit for pBR322 complexed with GP32 is shown in fig. 6. The radius of gyration of the pBR322 complex which can be calculated from this set of parameters does not fully agree with the experimental value (Rouse-Zimm model: $R_g = 184$ nm, while the experiments indicate that R_g is 141 nm). However, in view of the uncertainties in the static/dynamic light scattering experiment (10% error) and, more importantly, the approximations made in the Rouse-Zimm model, the disagreement may not be too serious. We note that if the value of R_g is chosen closer to the experimental value, no reasonable description of the D_{app} versus q^2 curve could be obtained. It was not possible to describe the D_{app} curves of the linear DNA–protein complex with the ISMF model, although this model does not contain any assumptions concerning the molecular topology except for the radius of gyration.

On the other hand the Rouse-Zimm model cannot be usefully applied to the results obtained for the circular DNAs since this model never predicts a plateau for small values of q^2. Therefore the ISMF model is the simplest model that can fit the data for the circular DNAs. Although it is again possible to describe the data, also in this case the fit parameters do not yield the correct radius of gyration. Alternatively, if we tried to describe the D_{app} curve for the circular DNAs with the ISMF model using the experimentally determined radius of gyration, the model curves showed a broad plateau at large q^2 in contrast with our observations. An example of such a 'fit' is given in fig. 7.

The model given by Soda [16] can be used to describe the D_{app} versus q^2 curves for a circular structure; however, due to computer-time limitations we were not able to generate a minimized fit of the D_{app} curve with the Soda model and only show some representative curves for different values of persistence length. In fig. 8 we show the predictions of the Soda theory and the data points for M 13 DNA complexed with GP32, using a diameter of 6 nm and a contour length of 2820 nm, while we varied the persistence length between 20 and 30 nm with 5 nm steps. We notice

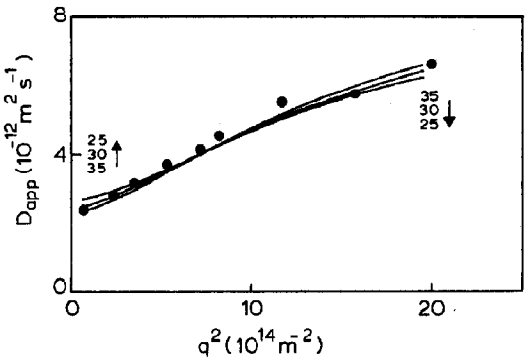

Fig. 8. The apparent diffusion coefficient versus q^2 calculated from autocorrelation functions that were generated using the Soda theory. The drawn lines were obtained using a contour length of 2820 nm, a diameter of 6 nm and the indicated persistence length in nm. For comparison of data points obtained for M 13 DNA complexed with GP32 are included in this figure (see text).

that the Soda model correctly predicts a 'flat' D_{app} curve for small values of q^2, for low values of the persistence length.

4.6. Global analysis

For each DNA–protein complex a global analysis was performed on four autocorrelation functions measured at different scattering angles, using the linear or circular free draining Rouse-Zimm expression and the ISMF expression as a theoretical model. The sum R as described in eq. 3 was minimized using eq. 5 with an appropriate choice of an A_i function. Since no a priori knowledge exists of the value of N this parameter was varied and $N = 10$, 20, 30 or 40 was chosen. A typical example of the global analysis, including the residuals, is shown in fig. 9 for the M 13–GP32 complex. Some of the results for the DNA–protein complexes are given in table 3.

For the pBR322–GP32 complex the value of R did not depend much on the actual choice of N (data not shown). Moreover, for this DNA–protein complex the value of R did not differ significantly for the linear Rouse-Zimm model and the ISMF model. For the M 13–GP32 complex the value of R indicated that the ISMF model describes the autocorrelation functions somewhat better, whereas in the case of M 13mp 10 the circular Rouse-Zimm model must be slightly preferred over the ISMF model. In conclusion, the residuals of the global analysis do not clearly favour one of the discrete models used.

Both the ISMF model and the Rouse-Zimm model predict a value for the radius of gyration which was measured independently. If we assume that the global analysis should yield the experimentally determined radius of gyration it can be concluded that the number of subsegments must be less than 15 for pBR322, M 13 and M 13mp 10 complexed to GP32 if the Rouse-Zimm model is applied. For the ISMF model this number is about 14 for pBR322, 18 for M 13mp 10 and 24 for M 13 complexes. For both models, N values, that give approximately the correct value for R_g, yield D_0 and D_{plat} values that agree rather well with the experiment. Systematically it was found that the fits with the ISMF model yield lower values for D_{plat} than the circular and linear Rouse-Zimm model.

The value of kT/g found in the global analysis with the Rouse-Zimm model can be used to calculate a root mean square subsegment size. This value was found to be about 33 nm for pBR322 and M 13mp 10 and 41 nm for the M 13 DNA complex with GP32. These values are much lower than the values for double stranded $\phi 29$ DNA as reported by Schurr et al. [25] (110 nm), in agreement with our conclusion that the DNA–protein complexes are more flexible than double stranded DNA. The calculated numbers suggest that the DNA–protein complexes are about two to three times more flexible than double stranded DNA.

In summary, both the ISMF model and the Rouse-Zimm model can reasonably describe the measured autocorrelation functions. Additional information, for instance the value of the radius gyration, allows a choice of N, which gives a D_0, kT/f and kT/g that appear in reasonable agreement with other experimental results. All these calculations yield N values which are of order 20, indicating a chain element consisting of about 300 bases or about 30 bound proteins, which corresponds to about 120 nm. If a chain element must

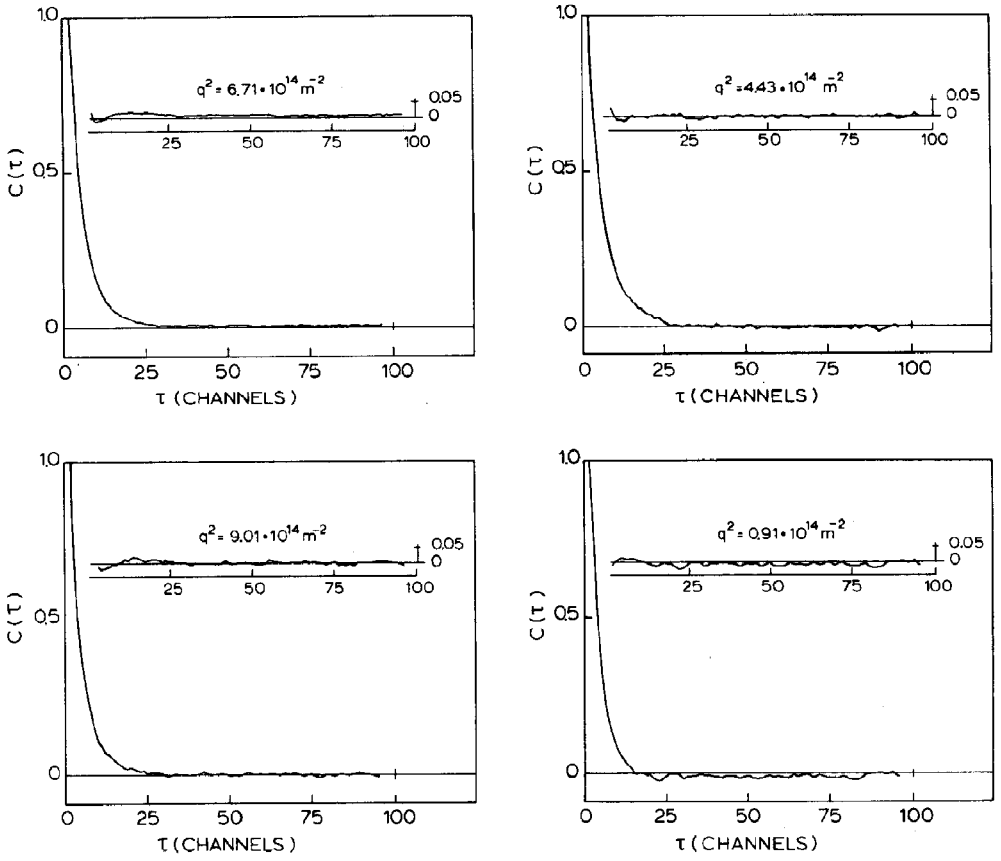

Fig. 9. Example of a global analysis of four autocorrelation functions obtained for M 13 DNA. The measured autocorrelation is shown after normalisation (raw amplitude ≈ 0.4) in every panel together with the residuals of the fit on the same vertical scale. The best parameters for this particular global analysis were $D_0 = 2.1 \times 10^{-12}$ m^2 s^{-1}, $kT/g = 0.67 \times 10^{-14}$ m^2, $kT/f = 2.9 \times 10^{-14}$ m^2 s^{-1} with $N = 15$ fixed.

Table 3

Results of the global analysis using $N = 20$

lrzc, linear Rouse-Zimm chain model eq. 7; crzc, circular Rouse-Zimm chain model eq. 8; ismf, independent segment mean force model eq. 6. Note: the value of the residuals R can only be compared for one type of DNA.

Type of DNA complexed with GP32	Model	kT/f (10^{-12} m^2 s^{-1})	kT/g (10^{-14} m^2)	D_0 (10^{-12} m^2 s^{-1})	R_g (nm)	R
Linear	lrzc	3.66	0.34	1.96	183	0.150
pBR322	ismf	3.50	0.74	2.08	149	0.151
Circular	crzc	3.97	0.48	2.13	220	0.044
M 13	ismf	3.26	0.92	2.28	166	0.022
Circular	crzc	3.87	0.36	2.00	190	0.013
M 13mp 10	ismf	2.98	0.70	2.07	145	0.019

consist of at least four persistence lengths [25], the maximum persistence length will be about 30 nm, in good agreement with the direct measurements. However, so far it is not clear whether these N chain elements represent structures that exist in reality.

5. Discussion

Until now the estimates of dimensions in solution of ss DNA complexed with GP32 were based on the properties observed in hydrodynamic experiments with small 145 base DNA fragments or transfer RNA [9]. In the present study we have chosen to extend the validity of the conclusions drawn in this earlier work to larger DNA–protein complexes, since in reality GP32 is assumed to occupy large stretches of ss DNA [33]. Moreover, we decided to estimate the rigidity of the GP32–DNA complexes since the flexibility of a template may play an important role in many of the processes in which GP32 is involved. For instance, the essential role of GP32 in repair processes suggests that very rigid structures are not favourable [34].

5.1. Absorbance measurements

Using absorbance spectroscopy it was shown that both large and small DNA–protein complexes give rise to very similar 'interaction' spectra. The spectrum of the M 13mp 10 complex is somewhat red-shifted compared to the 145 base complex spectrum, but this red-shift can also be observed in the spectra of the uncomplexed ss DNAs. A small difference in the amplitude of the 'interaction' spectrum was obtained, but within the experimental accuracy this difference cannot be ascribed to a different saturation of the DNAs with protein. Thus, from a spectroscopic point of view it can be concluded that the cooperative association of GP32 is identical for both small and large ss DNAs.

5.2. Sedimentation

It was shown that the 'hydrodynamic' size of the binding site can be obtained for large ss DNA–protein complexes and that the obtained values agreed reasonably well with the result obtained by Scheerhagen et al. [8] using the same approach with short DNA–protein complexes. However, it is also clear from our measurements that there are limitations to this approach. A strong dependence of D_{app} on q^2 at small q values will not yield an accurate value of D_0 and therefore a relatively large error in n. In addition very long DNA molecules such as λ DNA can easily break during the sample preparation.

All the measured values were below the number $n = 10$ reported by Scheerhagen et al. for the 145 base DNA complex, indicating that maybe in this latter case the 145 base DNA was not fully saturated. The measured n values were significantly above the values obtained by spectroscopic methods. Although the discrepancy is not too large, it is worthwhile to consider the intrinsic difference between the two types of measurement. The hydrodynamic method extracts information about the saturated DNA lattice and gives an upper bound for the size of the binding site. To determine the n value it is essential to know the length of the DNA molecule, the assumption that it is fully covered with protein and an estimate of the partial specific volume. The method is *not* sensitive for inactive protein. On the other hand, the spectroscopic method gives a lower limit since it is based on the assumption that *all* protein is active and gives the same optical changes upon binding until saturation is reached. Moreover, to obtain a numerical value for n, precise values for the extinction coefficients are needed (or some other measure for the concentration).

We do not believe that the partial specific volume of the complex is less than 0.7 cm^3/g. We also do not believe that the protein extinction coefficient is more than 5% off, in view of the fact that based on $\epsilon_{280} = 3.7 \times 10^4\ M^{-1}\,cm^{-1}$ Giedroc et al. found exactly one Zn-atom per GP32 [44,45]. We know from our own experience that extremely careful CD and absorbance titrations with poly(dT), poly(rA) or poly(rεA) as templates yield n values between 8–9 nucleotides covered by a protein monomer. These experiments have shown that the addition of GP32 to the nucleotide must be preferred, if low GP32 concentrations are used

in such measurements. In view of these considerations a choice of $n = 9 \pm 1$ seems to be consistent with most of the data.

5.3. Flexibility

To calculate the hydrodynamic properties of the 145 base DNA–protein complex Scheerhagen et al. used a rigid rod approximation [9]. This was partly based on the fact that the observed spectral properties of the GP32–DNA complexes were temperature independent, suggesting a regular and rigid structure of the complex [35]. Although the decay of the electric field induced birefringence of the 145 base DNA–protein complex showed at least two time constants, the salt, field strength and pulse-duration independence could not easily be explained in terms of flexibility [36]. Moreover, the dependence of the calculated length for several small RNA–protein complexes did not indicate a systematic decrease of the rise per base for longer complexes due to flexibility. Electron microscopy photographs have shown that the flexibility of long DNA complexed with GP32 must be comparable to the flexibility of double stranded DNA, and therefore the treatment of the complex as a rigid rod appeared to be justified [10]. The work presented here was specifically aimed at characterizing the dynamics of the DNA–protein complex, since in fact little is known about the actual flexibility in solution of this and other DNA–protein complexes. Several techniques have been applied to the dynamics of double stranded DNA yielding values for the bending persistence length [37–40]. In this work we focussed our attention on the sedimentation, light scattering and QELS properties of DNA–protein complexes.

5.3.1. Sedimentation as a probe for flexibility

The persistence length of double stranded DNA was obtained from the comparison of the sedimentation coefficient for a series of restriction fragments with different contour lengths [37]. The existence of a theory [41] that predicts the translational diffusion coefficient for flexible chains, dependent on the bending persistence length, allowed for an accurate determination of this parameter. However, the number of DNA lengths studied in our work certainly does not permit such an approach. However, from the theoretical expression given by Soda [16] a small angle translation diffusion coefficient can be calculated that agrees with the experimental value assuming a persistence length of about 30 nm and a rise per base of 0.44 nm. Of course, if n equals 9 ± 1 we obtain a sedimentation coefficient that also agrees with the experimental value.

5.3.2. Classical light scattering

The determination of the intra-particle interference function $P(\theta)$ from the scattered intensity of a macromolecular solution is commonly used to determine the radius of gyration, which is in turn determined by the flexibility of the macromolecule. A known complication is the excluded volume problem, which is ignored in the presentation of our results. It should be noted that if we include excluded volume effects the calculated persistence length will decrease. The principal aim of the classical light scattering experiments was to obtain a reasonable estimate of the radii of gyration and persistence lengths of the DNA–protein complexes. All complexes gave values for the persistence length that were smaller than the value found for double stranded DNA. In our view the bending persistence length is also small for the 145 base DNA–protein complex (M.E. Kuil et al., in preparation). Moreover, this relatively low value is probably not due to the fact that the DNA lattice is unsaturated (see above). These measurements imply that our notion of the DNA–protein complex as a relatively rigid and regular structure probably only reflects the local conformation due to one or at most a few proteins. Another remarkable conclusion that could be drawn is that the M 13mp 10 DNA–protein complex appears to be more flexible than the two others. This observation is also indicated by the obtained translational diffusion and sedimentation coefficients. However, if we combine the diffusion and sedimentation coefficient in the Svedberg relation we can show that this complex is equally saturated as compared to the other two and therefore this flexibility cannot be explained in terms of a contribution of naked pieces of DNA. Another possibility is that specific nucleotide sequences exist in

natural ss DNAs that give rise to this apparent high flexibility, for instance a small piece of double stranded DNA may be present that cannot be melted by GP32, thereby constraining the extension of the molecule. It will probably be worthwhile to study DNA–protein flexibility as a function of the sequence in selected DNAs.

5.3.3. Quasi-elastic light scattering

The measured auto-correlation functions of the light scattered at different angles by the DNA–protein complexes can be understood on the basis of a relatively flexible structure. It could be observed that the circular DNA–protein complexes showed a more constrained internal dynamics compared to the linear complexes, in line with similar experiments with linear, circular and supercoiled DNAs. The observed dynamics for the circular M 13 DNA, showing a more constrained internal dynamics, could be described with values for the persistence length and contour length that appear very realistic using the formalism given by Soda [16].

5.4. Model calculations

Global analysis of the scattered light autocorrelation functions showed that the introduction of an additional datum, the radius of gyration, was necessary to obtain a more reliable description of the data. Since there is no theory predicting the number of subsegments in a Rouse-Zimm chain, we needed additional information to decide on the choice of N. The choice of N based on the observed radius of gyration leads us to the same conclusion as the $P(\theta)$ calculations, namely that the DNA–protein complexes are characterized by a relatively small persistence length. If the DNA–protein complexes possess a significant bending flexibility the calculated rise per base is too low, and this value has to be reconsidered as already pointed out by Scheerhagen [11]. The adjusted (increased) rise per base lowers the value for the bending persistence length calculated in this work even further. In a forthcoming publication the implications of this low value for the persistence length on the solution dimensions of the complex of GP32 with short DNA fragments will be discussed (M.E. Kuil et al., in preparation).

Unfortunately, we were not able to implement the Soda theory in such a way that a global analysis could be performed using a reasonable amount of computer time. On the other hand, we were able to show that there must be a choice of parameters in the Soda model that both agree with the experiment and the results obtained with the other models.

Acknowledgements

This work was supported by a grant of the Netherlands Organization for the Advancement of Pure Research (N.W.O.). The authors are indebted to Dr. M. van Steenbergen (Dept of Oral Microbiology, Faculty of Dentistry, Free University, Amsterdam) for assistance in using the ultracentrifuge equipment. We wish to thank Mr. J. den Blaauwen for isolation of the 145 bp DNA, Mr. R.W. Visschers for help with the isolation of gene 32 protein and Mrs. B. Hoebee for advice and assistance with the preparation of plasmid DNA. We greatly appreciated the gift of M13 DNA from Dr. B.J.M. Harmsen (Dept of Biophysical Chemistry, Catholic University, Nijmegen).

References

1 S. Riva, A. Cascino and E.P. Geiduschek, J. Mol. Biol. 54 (1970) 85.
2 J.I. Tomizawa, N. Akaru and Y. Iwama, J. Mol. Biol. 21 (1966) 247.
3 S.C. Kowalczykowski, N. Lonberg, J.W. Newport and P.H. von Hippel, J. Mol. Biol. 145 (1981) 75.
4 R.C. Kelly and P.H. von Hippel, J. Biol. Chem. 251 (1976) 7229.
5 S.A. Anderson and J.E. Coleman, Biochemistry 14 (1975) 5485.
6 A.M. Bobst, P.W. Langemeier, P.E. Warwick-Koochaki, E.V. Bobst and J.C. Ireland, J. Biol. Chem. 257 (1982) 6184.
7 R.C. Kelly, D.E. Jensen and P.H. von Hippel, J. Biol. Chem. 251 (1976) 7240.
8 M.A. Scheerhagen, C.A. Vlaanderen, J. Blok and R. van Grondelle, J. Biomol. Struct. Dyn. 3 (1985) 887.
9 M.A. Scheerhagen, H. van Amerongen, R. van Grondelle and J. Blok, FEBS Lett. 179 (1985) 221.

10 H. Delius, N.J. Mantell and B. Alberts, J. Mol. Biol. 67 (1972) 341.
11 M.A. Scheerhagen, M.E. Kuil, R. van Grondelle and J. Blok, FEBS Lett. 184 (1985) 221.
12 M.A. Scheerhagen, M.E. Kuil, H. van Amerongen and R. van Grondelle, J. Biom. Struct. Dyn. (1988) in press.
13 H. van Amerongen, M.E. Kuil, F. van Mourik and R. van Grondelle, J. Mol. Biol. (1988) in press.
14 S.C. Lin and J.M. Schurr, Biopolymers 17 (1978) 425.
15 H. van Amerongen, R. van Grondelle and P.C. van der Vliet, Biochemistry 26 (1988) 4646.
16 K. Soda, Macromolecules 17 (1984) 2365.
17 K. Soda and A. Wada, Biophys. Chem. 20 (1984) 185.
18 J. Hosoda and H. Moise, J. Biol. Chem. 253 (1978) 7547.
19 T. Maniatis, E.F. Fritsch and T. Sambrook, Molecular cloning (Cold Spring Harbor Laboratory, Cold Spring Harbor, NY).
20 L.C. Lutter, J. Mol. Biol. 124 (1978) 391.
21 P.C. Hopman, Ph. D. Thesis (Free University, Amsterdam, The Netherlands, 1980).
22 M. Fujii and H. Yamakawa, Macromolecules 8 (1975) 792.
23 A. Peterlin, Makromol. Chem. 9 (1952) 244.
24 W.I. Lee and J.M. Schurr, Chem. Phys. Lett. 23 (1973) 603.
25 J. Wilcoxon and J.M. Schurr, Biopolymers 22 (1983) 2273.
26 J.C. Thomas, S.A. Allison, J.M. Schurr and R.D. Holder, Biopolymers 19 (1980) 1451.
29 O.G. Berg, Biopolymers 18 (1979) 2861.
30 S.N. Timasheff and R. Townend, in: Physical principles and techniques of protein chemistry part B, ed. S.J. Leach (Academic Press, New York, 1970), p. 158.
28 D.M. Crothers and B.H. Zimm, J. Mol. Biol. 12 (1965) 525.
29 O.G. Berg, Biopolymers 18 (1979) 2861.
30 R.B. Caroll, K.E. Neet and D.A. Goldthwait, Proc. Natl. Acad. Sci. U.S.A. 69 (1972) 2741.
31 G. Voordouw, Z. Kam, N. Borochov and H. Eisenberg, Biophys. Chem. 8 (1978) 171.
32 J. Langowski, U. Giesen and C. Lehmann, Biophys. Chem. 25 (1986) 191.
33 B.M. Alberts and L. Frey, Nature 227 (1970) 1313.
34 C.M. Radding, Annu. Rev. Biochem. 47 (1978).
35 M.A. Scheerhagen, J. Blok and R. van Grondelle, J. Biomol. Struct. Dyn. 2 (1985) 821.
36 M.A. Scheerhagen, Ph. D. Thesis (Free University, Amsterdam, The Netherlands, 1986).
37 R.T. Kovavic and K.E. van Holde, Biochemistry 16 (1977) 1490.
38 P.J. Hagerman, Biopolymers 20 (1981) 1503.
39 J.G. Elias and D. Eden, Macromolecules 14 (1981) 410.
40 J.E. Godfrey and H. Eisenberg, Biophys. Chem. 5 (1976) 301.
41 H. Yamakawa and M. Fujii, Macromolecules 6 (1973) 407.
42 D.E. Jensen, R.C. Kelly and P.H. von Hippel, J. Biol. Chem. 251 (1976) 7215.
43 J. Newman, H.L. Swinney, S.A. Berkowitz and L.A. Day, Biochemistry 13 (1974) 4832.
44 D.P. Giedroc, K.M. Williams, K.R. Koningsberg and J.E. Coleman, Proc. Natl. Acad. Sci. U.S.A. 83 (1986) 8452.
45 K.M. Keating, L.R. Ghosaini, D.P. Giedroc, K.R. Williams, J.E. Coleman and J.M. Sturtevant, Biochemistry 27 (1988) 5240.
46 H. van Amerongen and R. van Grondelle, submitted for publication in J. Mol. Biol. (1988).